Evaluation of an electrochemical cell 3D-printed
with PLA/PTFE polymer filament

A. Márquez-Herrera[a,*], and M. Zapata-Torres[b] and S. Montesinos[c]

[a]*Departamento de Ingeniería Agrícola, División de Ciencias de la Vida,*
Campus Irapuato-Salamanca, Universidad de Guanajuato, Irapuato, Guanajuato 36500, México.
[*]e-mail: amarquez@ugto.mx
[b]*Centro de Investigación en Ciencia Aplicada y Tecnología Avanzada,*
Unidad Legaria, Instituto Politécnico Nacional, Ciudad de México, 15000, México.
[c]*Departamento de Ingeniería Industrial, Universidad Tecnológica de la Mixteca,*
Huajuapan de León, Oaxaca 69000, México.

3-dimensions (3D) printing technology is a type of additive manufacturing (AM) that is on the rise and works by manufacturing components by the deposition of a thermoplastic layer upon layer. In this paper, we explore the use of AM to print a novel fused deposition modeling-based 3D printing electrochemical cell from a non-commercially available composite of PLA/PTFE polymer filament for corrosion applications within materials science. To validate the 3D printed cell, a galvanic series and cyclic voltammetry to aluminum in Hank's solution was done, and a corrosion resistance study was conducted by using the electrochemical impedance spectroscopy (EIS) and anodic and cathodic polarization (Tafel) techniques to a virgin and a boride ASTM F-73 alloy as working electrode. The results show the possibility of replacing commercial electrochemical cells with 3D printed ones without any compromise on quality of the experiment. Also, this inexpensive and simple instrument design is both, adaptable and sensitive for a wide range of laboratory electrochemical applications.

Keywords: 3D-Printing; PLA/PTFE; filament; electrochemical cell.

1. Introduction

Corrosion is a natural process which mainly degrades metals due to electrochemical reactions because these materials are trying to reach their lower energy potential state. Corrosion has many implications in terms of security concerns, preservation of materials, and economic issues, so its study and mitigation are highly important. In this context, engineers must have a solid understanding of the chemical and physical bases of corrosion, as well as an understanding of the engineering issues about corrosion. Due to this, corrosion topics are included in many courses in the educational program of most bachelor's degree curriculums and associated engineering fields, and in many other programs. In this sense, the three-electrode cell is the standard laboratory apparatus for the quantitative investigation of the corrosion properties of materials, however its high cost restricts the infrastructure available for laboratory research or education activities. As a result, most bachelor-level graduates of materials and design related programs have an inadequate background in corrosion engineering practices and principles. For example, in México where its public institutions live with budgetary restrictions, commercial electrochemical cells, usually made of glass, imply a high cost for laboratory equipment. Also, its construction is a labor-intensive process that requires skilled workshop techniques such as cutting, milling, and drilling. Its design is tedious and costly in terms of labor, materials, and time. Fortunately, 3D printing is a group of fabrication methods to build objects with desired shapes, sizes, and functionalities [1–4]. The most common 3D printing method is fused deposition melting (FDM). FDM requires low operational expenditure and capital and involves safe materials, making it an ideal rapid prototyping tool for electrochemical laboratories. Designing and using 3D-Printed prototypes allow students or researchers to manufacture, adaptable, cheap, disposable, and reliable electrochemical cells. Although educational institutions have greater access to computer aided design (CAD) software and 3D printers which the low cost fabrication of electrochemical devices may become more accessible to researchers and students, unfortunately we did not find any references on the proper usage of 3D-printing PLA filaments to fabricate electrochemical cells for serving to research the corrosion properties for materials science [5]; thus, this paper fills in that niche. In the current work, additive manufacturing (AM), also known as 3D printing, was used for manufacturing an electrochemical cell on a low cost 3D printer. Additionally, the printed cell was validated using aluminum (Al) as a common material and the result was compared with experiment using a commercial cell. Due this topic is most effectively explored in the laboratory to investigate complex phenomena within an applied and relevant context, also the cell was evaluated by using a biomedical material as ASTM F-75 (CoCrMo) alloy. Although the experiments in this work can be used as part of the teaching practice for students, the study is limited to presenting a device that can be used for laboratory learning and some research activities.

FIGURE 1. Homemade 3D filament extruder.

2. Materials and methods

2.1. The 3D-printed cell

The electrochemical cell was designed in SolidWorks software and then converted into a stereolithog-raphy (stl) digital format suited to 3D printer. The cell was printed using an Ender 3 Pro 3D Printer from Shenzhen Creality 3D Technology Co., Ltd. To print the electrochemical cell was used a thermoplastic polymer (PLA/PTFE) filament that was formulated with 97 wt.% polylactic acid (PLA) polymer and 3 wt.% polytetrafluoroethylene (PTFE) [6]. PLA pellets and PTFE powder were mixed at 100 rpm during 1 h in methylene chloride solvent using a magnetic stirrer. Then the solution was placed in a drying oven at 60 °C for 24 h and then the final material was cut in small pieces. To obtain the filament, the PLA/PTFE blends were extruded using homemade single-screw extruder at 215 °C, as shown in Fig. 1

2.2. The 3D-printed cell validation for laboratory learning

To validate the 3D-printed electrochemical cell, it was covered the development of a galvanic series and also a single cyclic voltammetry test to aluminum, as model, immersed in a Hank's solution as electrolyte, and then compared against the results obtained from a commercial cell K0235 flat cell kit from AMETEK Scientific Instruments, Inc. under the same conditions. When two different metals in electrical contact are bared to same electrolyte, one of the metals can show a decreased corrosion while the other can undergo increased corrosion. This kind of accelerated corrosion is named as galvanic corrosion [7]. One method that is used to predict the effects of galvanic corrosion is to establish a galvanic series by arranging a list of the materials of interest to measure corrosion potentials in the environment and under conditions of interest. Each series is specific to the environment for which it was arranged. In this case, the galvanic series of aluminum was done by the open circuit potential (OCP) under

the standard ASTM G82-98 (2014). Although the development of the galvanic series, as well as many others, is often a common laboratory practice for students, additionally this comparison would demonstrate the validity of using the 3D-printed cell for corrosion studies by showing that results are equal. Finally, cyclic voltammetry is a technique where the potential between two electrodes is varied while the current is measured. Since measured current response is dependent on the concentration of the redox species (the analyte) and electrodes, it would be expected that the voltammetry curve would be equal in any cell under the same conditions [8].

2.3. The 3D-printed cell validation for research activities

Boride, also named boronizing, is a thermochemical process where boron is diffused into the alloy or metal surface. The resulting surface contains metal borides, and these borides usually have a high wear resistance and extremely high hardness [9]. To evaluate the cell for research activities, a novel study of corrosion on virgin and boride alloy samples was conducted. So, a boride biomedical ASTM F-75 (CoCrMo) alloy was used as a working electrode with about 25 mm diameter × 5 mm thickness. The samples were polished by using SiC sandpaper from 240 to 1200 grit, and then by diamond paste until a mirror finish was achieved. The boriding process involved deposition of boron paste (consisted of 5 wt.% B_4C powder as a source of boron, 5 wt.% KBF_4 as a flux and 90 wt.% SiC as refractory material) above substrate to form about 5 mm thickness layer. The coated alloy sample was then placed in a preheated muffle furnace at 950 °C during 4 h. The crystal phase structure of the samples was analyzed by X-ray diffraction (XRD). The corrosion study was done by the electrochemical impedance spectroscopy (EIS) and polarization technique (Tafel). Hank's solution was used as simulated body fluid to characterize the metallic biomedical CoCrMo alloy. An open circuit potential (OCP) was applied for 3600 s before each corrosion measurement. A sinusoidal alternating current (AC) signal of 10 mV, scanning from 100000 Hz to 25 mHz, was applied for the impedance test. The Tafel plots were obtained by performing ± 150 mV scan vs. corrosion potential (Ecorr) at a scan rate of 0.5 mV/s to find both Icorr (corrosion current) and Ecorr. After performing E and (logarithmic scale) log I measurements, both anodically and cathodically polarized, a practical method to determine the corrosion current (Icorr) is superimposed a straight line along the linear portion of the anodic and cathodic curve and then the extrapolated linear portions of the anodic and cathodic polarization should intersect at the value corresponding to log Icorr and Ecorr. A minimum of three samples for each set of experimental parameters was exposed to the tests and compared with a sample that was not coated with boron (unboride sample). Also, the experiments were always repeated several times for each sample to test the reproducibility of results.
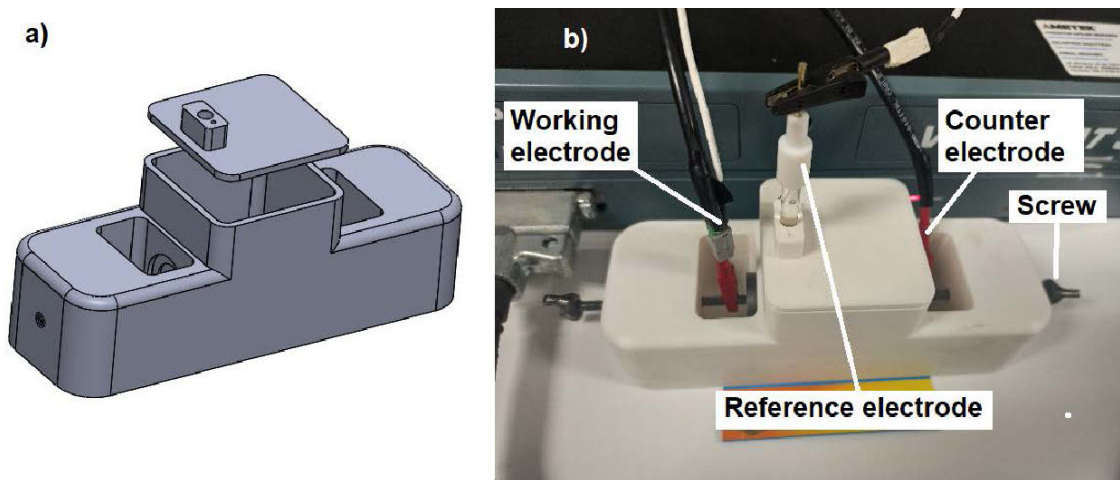
FIGURE 2. a) CAD SolidWorks model assembly for the electrochemical cell. b) Complete electro-chemical design made via 3D printing using PLA and PTFE polymer.

3. Results and discussions

Figure 2 shows a view of the 3D-printed electrochemical cell.

The printed cell has a size of 180 mm length, 60 mm width and 60 mm height. The middle compartment or container has a volume of about 169 mL that holds the electrolyte solution, providing an exposed electrode area of 1 cm^2. Figure 3 shows a cut view of the 3D-printed electrochemical cell. The provided cut view shows the internal features.

An important element for any type of electrochemical cell is the counter electrode (CE) [10]. It provides a means of applying an input potential to the working electrode. The purpose of this electrode is to complete the circuit and allow charge to flow. Consequently, it must be built from an inert material to ensure no current limitations arise. In this sense, the use of platinum (Pt) is preferable as a counter electrode due to the advantages it presents, however it is very expensive. 3D printing allows for adapting the design of an

FIGURE 3. Cut view of the complete electrochemical design made via 3D printing.

electrode at the lowest possible price. As the counter electrode, Fig. 2, a platinum foil of 0.1 mm thickness and 99.9 % wt. purity, so reducing its price, was used. Another cheaper option can be dental platinum foil. To promote a good seal between the counter electrode and the cell, a backing plate (such as copper, titanium, stainless steel, etc.) was joined to the platinum foil by silver solder paste; as it is shown in Fig. 3, the Pt is mounted such that the material of the backing plate is not exposed to solution but hold Pt steady; a commercial Ag/AgCl (3M KCl) reference electrode (RE) was used to measure the electrode potentials. Figure 3 shows a representation of virgin polytetrafluoroethylene (PTFE) gaskets which were used between the electrodes and the compartment to seal the cell. Due the electrochemical reactions inside any electrochemical cell, it cannot be completely covered, so the top lid has a vent hole to allow degassing. The first reported applications of fused deposition melting (FDM) in the electrochemical research include building reaction cells for water electrolysis [11], cells for spectro-electrochemistry [12], as well as the construction of electrochemical flow cells [13, 14], printed conductive metallic objects serving as electrodes [15], electrochemical sensors [16] and reference electrodes [17]. Although, several similar designs are available in published works as those mentioned, or for example thingiverse, many of them do not show any validation or consider the material degradation [12–17]. Others have sought to reduce the degradation of PLA by mixing it with other materials [18], doing a thermal or chemical treatment or just using other material [11, 19, 20]. In general, PLA is more resistant to degradation than other biodegradable polymers. While the primary condition to obtain substantial biodegradation of PLA is a higher temperature than the glass transition temperature of PLA [21], most of the electrochemical tests are limited to room temperature, as in this case, so temperature does not limit the use of this material for the construction of an electrochemical cell. However, hydrolytic degradation is a critical first step in the biodegradation of PLA where its ma-
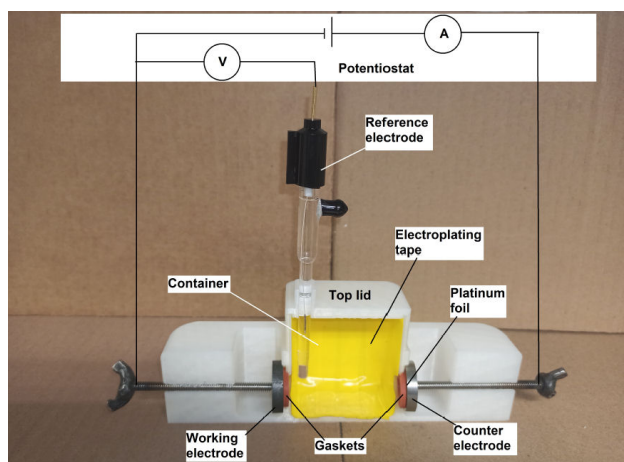
jor hydrolytic degradation rate starts after 20 days [22], so its use in an aqueous solution should be taken account. A factor that could limit the use of PLA is the type of solution to be used, in this sense the solution pH must be considered. Some works [23–25] show that although the material can be used in solutions with a pH between 3 and 13, it degrades very slowly in acidic solution (pH 3,0) while the degradation is faster at pH 8,0 or higher. The contact of PLA with solution could change the solution pH affecting the electrochemical measurements, in this case the material was mixed with PTFE and the compartment was covered by a mask tape, as shown in Fig. 3. The mask tape is fabricated from commercial electroplater's tape as JVCC VEPT-65 vinyl electroplating tape (there are another brands as 3M model 470 tape). This kind of tape incorporates a special adhesive to bond aggressively to material surface to discourage underflow of the tape edge by the electrolyte, which would cause degradation to the material. The tape is formulated to withstand lengthy exposure to chemicals commonly found in electrochemical applications. When it is necessary, the tape is removed and discarded. It is important to point out that the flexibility offered by 3D printing allows the production of complex electrochemical cell designs which can be profiled and sized and potentially realized in a single and facile process, decreasing the quantity of labor, raw material, and cost. Additionally, 3D printing allows the use of other thermoplastic filaments. Despite the cell, shown in Fig. 2, is an one experiment design, it can be adapted or redesigned for other electrode geometries, for example, a curved surfaces.

Figure 4 shows the X-ray diffractogram of the aluminum (Al), used to develop the validation of cell. The positions of the diffraction peaks associated with the crystal structure of Al, obtained respectively of entry number 96-901-2003 from the Crystallography Open database (COD) [26], are also shown. Hence, according to the X-ray diffractograms, the material is aluminum.
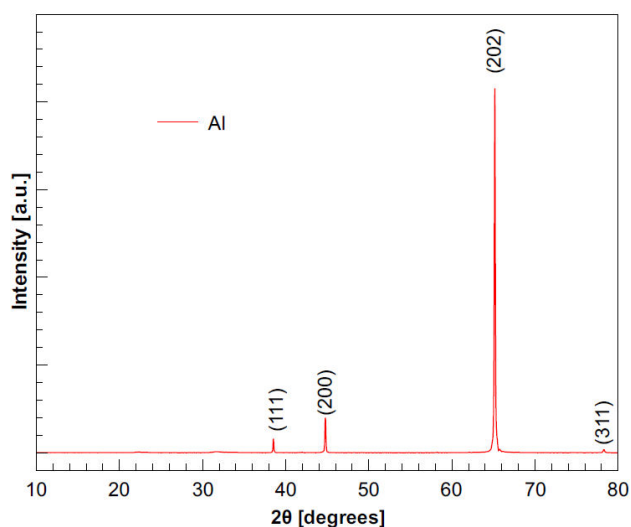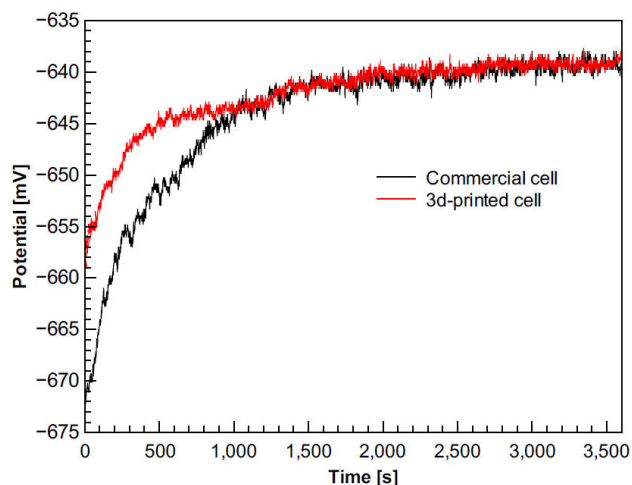

FIGURE 5. Open circuit of aluminum in hank's solution.

Figure 5 shows the open circuit curves of aluminum in the 3D-printed and commercial cell, respectively. These results shown that each cell reproduces the galvanic series of aluminum reported in literature. It means that the 3D-printed can be used in corrosion studies.

Although cyclic voltammetry has been used for electrode testing where well-defined voltammograms are produced when electrodes are working properly [17], in this study voltammetry is used for cell testing. The 3D-printed cell was measured against a commercial cell under the same conditions to validate it. The voltammetry experimental conditions were designed in the light of Gómez-Figueroa *et al.* [8]. Figure 6 shows cyclic voltammograms of aluminum using a commercial and 3D-printed cell in Hank's solution.

Figure 6 shows well-defined voltammograms that were produced with the use of the same reference electrode and solution. Although the figure shows a little shift in the 3D-printed cell values, this could be due that distances between

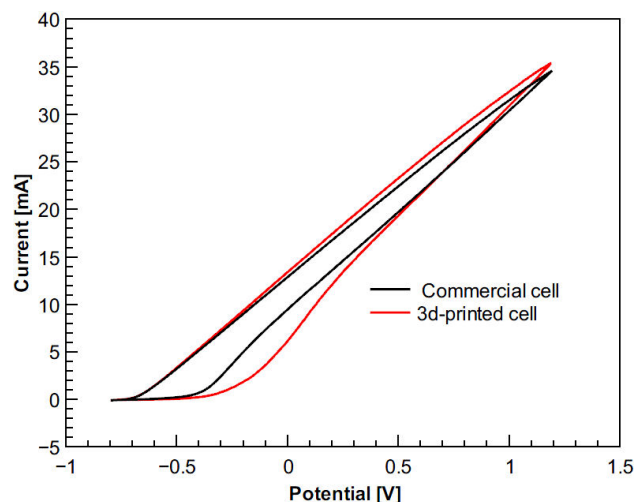FIGURE 4. X-ray diffraction patterns of aluminum sample.

FIGURE 6. Representative cyclic voltammograms of aluminum using a commercial and 3D-printed cell in Hank's solution. Initial potential = -0.8 V, vertex potential = 1.2 V, final potential = -0.8 V, scan rate = 250 mV/s.
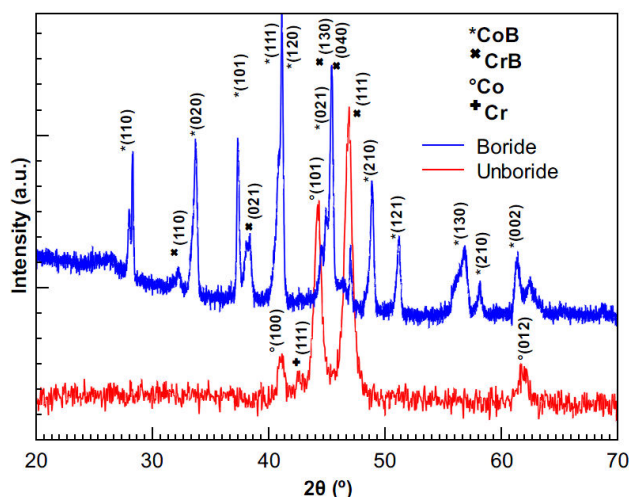
FIGURE 7. X-ray diffraction patterns of unboride and boride sample.

FIGURE 9. Complex impedance curves for unboride and boride samples in Hank's solution using the 3D-printed cell.
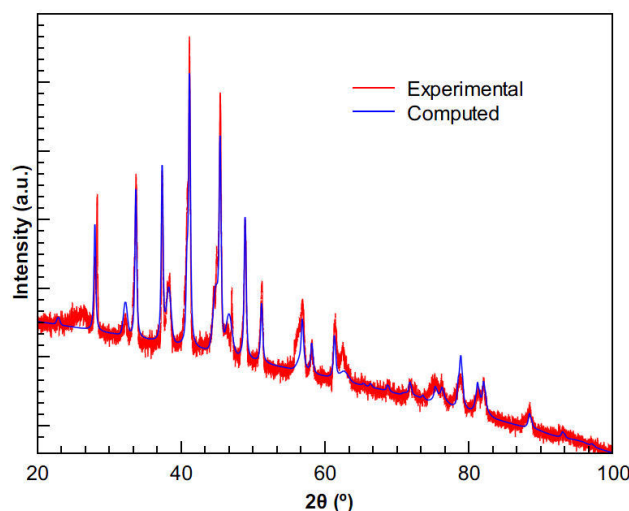

FIGURE 8. X-ray diffractogram of the boride sample. Also, XRD spectra as fitted by the Rietveld refinement program.

the working electrode and the counter electrode of both cells are different. When there is a greater distance between working and counter electrode, there will be a greater electrolytic resistance and therefore there will be a lower current [27]. However, the variation in measurements is not significant enough to distinguish a difference in performance of the 3D-printed cell when compared with the commercial cell, meaning that cell is appropriate for electrochemical measurements. Once the validity of the cell is shown and because the laboratory practices for students are limited to room temperature, non-corrosive and non-dangerous solutions, the cell can be used in a relevant way in education. Regarding research activities, Fig. 7 shows the X-ray diffractogram of the unboride and boride samples, second experiment. The positions of the diffraction peaks associated with the crystal structure of CoB and CrB, obtained respectively from 9008945 and 9008948 cards from the Crystallography Open database (COD), are
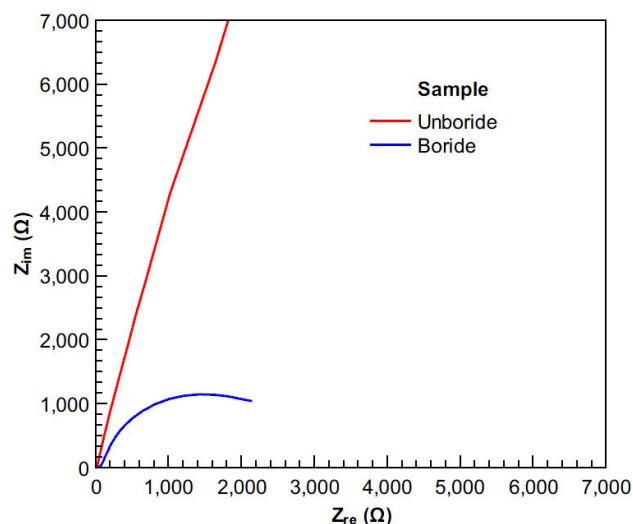
also shown. Hence, according to the X-ray diffractograms, the boride layer is composed of CoB and CrB crystals.

The phase percentages in the boride layer of the boride sample were determined according to the Rietveld refinement method [28] using the Maud software [29]. Figure 8 shows the X-ray diffractogram of the boride sample as fitted by the Maud software. With a weighted profile R-factor (RWP) of about 3.8 %, the phase percentages found for the boride layer sample were about 72.8 % and 27.2 % for CrB and CoB, respectively.

It is important to note that there is formation of borides only on the surface layer. Although the Rietveld refinement highlights the presence of MoB, it is not reported here because it is within the error of the technique. To evaluate the effect of the boride layer in the corrosion resistance of ASTM F-75 alloy sample using the 3D-printed cell, the polarization curves (Tafel) and Nyquist diagrams (EIS) were used. Figure 9 shows the results obtained by EIS (Nyquist plot).

Figure 9 shows that projection of the boride sample impedance (x-axis) is significantly lower than that of the unboride sample. As a first approximation, these results suggest that the boride process over the alloy provides a lower biocompatibility than the virgin ASTM F-75 alloy.

Figure 10 shows the Tafel curves of the unboride and boride samples using the 3D-printed cell, while Table I shows the values of corrosion potential (Ecorr) and corrosion current (Icorr) obtained from the polarization curves.

Table I shows that the exchange current density at the interface for the sample subjected to boride annealing is lower than that of the unboride sample: this manifests as a decrease in the corrosion current, Icorr. By comparison, these results confirm that the boride diffusion layer does not protect the alloy from chemical reaction of ions like the virgin material, suggesting that boride ASTM F-75 alloy is not a good candidate for biomedical applications as other authors have stated [30–36]. Also, these results agreed with a previously
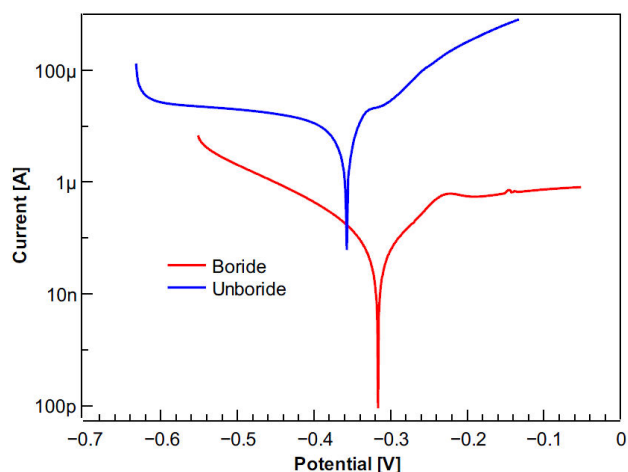
FIGURE 10. Tafel curves in Hank's solutions of unboride and boride alloy using the 3D-printed cell.

TABLE I. Summary of results obtained from corrosion tests performed in Hank's solution.

Sample	Ecorr (mV)	Icorr (μA)
Unboride	-318,3	0,07
Boride	-254,5	2,42

published work conducted by using a commercial K0235 Flat Cell Kit from AMETEK Scientific Instruments, Inc. [37].

4. Conclusions

We developed a simple, three-dimensional, model of a complete electrochemical cell that provides useful insight into the corrosion mechanism and its effect on the materials' performance. Also, this work demonstrates how the 3D-printing technology can be used to produce simple 3D-printed electrochemical cells for corrosion measurements in materials science using PLA/PTFE filament. Aditionally, the hydrolytic degradation is limited by coating the container using a commercial electroplating tape. The electrochemical cell was evaluated by conducting a corrosion study over unboride and boride ASTM F-75 alloy where the boride sample in a corrosive en-vironment employing Hank's solution exhibits inferior corrosion resistance compared to the unboride sample. While increase popularity in the research literature, the combination of 3D-printing and CAD also offers a new method for developing innovative designs for the electrochemical laboratory. Although this cell is an one experiment design, it can be adapted or redesigned for other geometries. This electrochemical cell will be beneficial for students, researchers and laboratories that require low-cost devices to reduce the operating cost of electroanalytical experiments. Finally, it can be concluded that this study provides further scope for research into the possibilities of replacing commercial electrochemical cells and devices with 3D-printed non-metallic ones, due to the rising costs and dwindling resources to sustain the same utility of product without any compromise on durability, reliability, and quality.

Acknowledgements

1. C. Alexandru-Polifron, B. Paul-Petru, R. Rradu-Iulian, and D. Liliana, Aspects Regarding the Use of 3D Printing Technology and Composite Materials for Testing and Manufacturing Vertical Axis Wind Turbines, *Mat. Plast.* **56** (2019) 910-917. https://doi.org/10.37358/MP.19.4.5283.

2. Y. Bozkurt, and E. Karayel, 3D printing technology; methods, biomedical applications, future opportunities and trends , *Journal of Materials Research and Technology* **14** (2021) 1430-1450. https://doi.org/10.1016/j.jmrt.2021.07.050.

3. M. S. Thompson, Current status and future roles of additives in 3D printing-A perspective, *Vinyl Addit. Technol. 1* (2022). https://doi.org/10.1002/vnl.21887.

4. G. Kasap, Y. D. Gokdel, M. B. Yelten and O. Ferhanoglu, Reliability Testing of 3D-Printed Polyamide Actuators, *in IEEE Transactions on Device and Materials Reliability* **20** (2020) 152-156. https://doi.org/10.1109/TDMR.2020.2966043.

5. A.L. Silva, S.G. Maia-Da-Silva, V.F. Castro-Silvia, M.F. Carvalho-Nakédia, and A. Munoz-Rodrigo, 3D printer guide for the development and application of electrochemical cells and devices, *Frontiers in Chemistry* **9** (2021) 1-19. https://doi.org/10.3389/fchem.2021.684256.

6. A. Márquez-Herrera, Extrusion parameters to obtain PLA/FTPE thermoplastic polymer filament , to be published.

7. F. León-Bello, and M. G. Amaya-Malpica, Surface galvanic action on a carbon steel matrix microcell consisting on ferrite and pearlite grains, *Rev. Mex. Ing. Quím.* **7** (2020) 29-33.

8. A. Gómez-Figueroa, Evaluación de la protección a la corrosió en el acero de refuerzo implementando recubrimientos a base de nanotubos de carbono adicionado con Zinc NTC-Zn como protección catódica , Thesis de Maestría en Construcción, Instituto Tecnológico de Chetumal, México.

9. A. Márquez-Herrera, and J. Moreno-Palmerin, Corrosion resistance evaluation of boron-carbon coating on ASTM A-36 steel, *Rev. Mex. Fís.* **68** (2022) 1-6. https://doi.org/10.31349/RevMexFis.68.011001.

10. K. C. Honeychurch, 13-Printed thick-film biosensors, In Woodhead Publishing Series in Electronic and Optical Material , Printed Films, Woodhead Publishing: Cambridge, UK. (pp. 366-409).

11. G. Chisholm, P. J. Kitaon, N. D. Kirkaldy, L. G. Bloor, and L. Cronin, 3D printed flow plates for the electrolysis of water: an economic and adaptable approach to device manufacture , *Energ. Environ. Sci.* **7** (2014) 3026-3032. `https://doi.org/10.1039/C4EE01426J`.

12. E. Achilli *et al.*, 3D-printed photo-spectroelectrochemical devices for in situ and in operando X-ray absorption spectroscopy investigation , *J. Synchrotron. Radiat.* **23** (2016) 622, `https://doi.org/10.1107/S1600577515024480`.

13. G. W. Bishop *et al.*, 3D printed fluidic devices for nanoparticle preparation and flow-injection amperometry using integrated Prussian Blue nanoparticle-modified electrodes, *Anal. Chem.* **87** (2015) 5437-5443. `https://doi.org/10.1021/acs.analchem.5b00903`.

14. C. P. De-León *et al.*, The 3D printing of a polymeric electrochemical cell body and its characterization, *Chem. Eng. Trans* **4** (2014) 2014.

15. E. Vaneckova *et al.*, UV/VIS spectroelectrochemistry with 3D printed electrodes, *Journal of Electroanalytical Chemistry* **857** (2020) 113760. `https://doi.org/10.1016/j.jelechem.2019.113760`.

16. R. M. Cardoso *et al.*, 3D printing for electroanalysis: From multiuse electrochemical cells to sensors , *Analytica Chimica Acta*, **1033** (2018) 49-57. `https://doi.org/10.1016/j.aca.2018.06.021`.

17. B. Schmind, D. King, and J. Kariuki, Designing and Using 3D-Printed Components That Al-low Students To Fabricate Low-Cost, Adaptable, Disposable, and Reliable Ag/AgCl Reference Electrodes , *J. Chem. Educ.* **95** (2018) 2076-2080. `https://doi.org/10.1021/acs.jchemed.8b00512`.

18. H. García-Cruz, M. Jaime-Fonseca, E. Von Borries-Medrano, and H. Vieyra, Extrusion parameters to produce a PLA-starch derived thermoplastic polymer , *Revista Mexicana De Ingeniería Química* **19** (2020) 395-412. `https://doi.org/10.24275/rmiq/Poly1529`.

19. P. B. Michelle, U. Veronika, P. Jan, N. Filip, and P. Martin, Inherent impurities in 3D-printed electrodes are responsible for catalysis towards water splitting , *Journal of Materials Chemistry A* **8** (2020) 1120-1126. `https://doi.org/10.1039/C9TA11949C`.

20. P. Alves-Ferrerira *et al.*, Multi sensor compatible 3D-printed electrochemical cell for voltammetric drug screening , *Analytica Chimica Acta* **1169** (2021). `https://doi.org/10.1016/j.aca.2021.338568`.

21. S. Teixeira, K. M. Eblagon, F. R. Miranda, M. F. Pereira, and J. L. Figueiredo, To-wards controlled degradation of Poly(lactic) Acid in technical applications, *C* **7** (2021) 1-43. `https://doi.org/10.3390/c7020042`.

22. F. Zuluaga, Algunas aplicaciones del ácido poli-L-láctico , *Revista de la Academia Colombiana de Ciencias Exactas, Físicas y Naturales* **37** (2013) 125-142.

23. S. Lazzari, F. Codari, G. Storti, M. Morbidelli, and D. Moscatelli, Modeling the pH-dependent PLA oligomer degradation kinetics . *Polymer Degradation and Stability* **110** (2014) 80-90. `https://doi.org/10.1016/j.polymdegradstab.2014.08.012`.

24. X. Lebo, C. Kaitlyn, and B. G. Christipher, Effects of Temperature and pH on the Degradation of Poly(lactic acid) Brushes , *Macromolecules* **44** (2011) 4777-4782. `https://doi.org/10.1021/ma2000948`.

25. L. Yuechi, G. Meiyu, S. Dusita, F. Johannes, and B.S. Gleb, pH dependent degradation properties of lactide based 3D microchamber arrays for sustained cargo release , *Colloids and Sur-faces B: Biointerfaces* **188** (2020) 1-8. `https://doi.org/10.1016/j.colsurfb.2020.110826`.

26. A. Merkys, A. Vaitkus, J. Butkus, M. Okulic-Kazarinas, V. Kairys, and S. Grazulis, COD::CIF::Parser: an error-correcting CIF parser for the Perl language , *Journal of Applied Crystallography* **49** (2016) 292-301. `https://doi.org/10.1107/s1600576715022396`.

27. G. Reade, G. Ottewill, and F. Walsh, Understanding electrical and electrolytic conductivity , *Trans. IMF.* **78** (2000) 89-92.

28. H. M. Rietveld, Line profiles of neutron powder-diffraction peaks for structure refinement , *Acta Cryst.* **22** (2007) 151-152.

29. L. Lutterotti, M. Bortolotti, G. Ischia, I. Lonardelli, H. R. Wenk, Rietveld texture analysis from diffraction images , *Z. Kristallogr. Suppl.* **26** (2007) 125-130. `https://doi.org/10.1524/9783486992540-020`.

30. I. Campos-Silva *et al.*, Growth kinetics and mechanical properties of boride layers formed at the surface of the ASTM F-75 biomedical alloy, *Surface & Coatings Technology* **237** (2013) 402-414. `https://doi.org/10.1016/j.surfcoat.2013.06.083`.

31. M. Dong, and S. Bao-luo, Oxidation resistance of boronized CoCrMo alloy , *International Journal of Refractory Metals and Hard Materials* **28** (2010) 424-428. `https://doi.org/10.1016/j.ijrmhm.2010.01.003`.

32. J. M. Johnston, M. Jubinsky, and S. A. Catledge, Plasma boriding of a cobalt-chromium alloy as an interlayer for nanostructured diamond growth , *Applied Surface Science* **328** (2015) 133-139. `https://doi.org/10.1016/j.apsusc.2014.11.129`.

33. M. Dong, S. Bao-luo, and Z. Xin, Effects of boronizing on mechanical and dry-sliding wear properties of CoCrMo alloy , *Materials and Design* **31** (2010) 3933-3936. `https://doi.org/10.1016/j.matdes.2010.03.024`.

34. M. Metikos-Hukovic, Z. Pilic, R. Babic, and D. Omanovic, Influence of alloying elements on the corrosion stability of CoCrMo implant alloy in Hank's solution , *Acta Biomaterialia* **2** (2006) 693-700. `https://doi.org/10.1016/j.actbio.2006.06.002`.

35. I. Campos-Silva *et al.*, The boriding process in CoCrMo alloy: Fracture toughness in cobalt boride coatings , *Surface & Coatings Technology* **260** (2014) 362-368. `https://doi.org/10.1016/j.surfcoat.2014.07.092`.

36. G. A. Rodríguez-Castro *et al.*, Micro-abrasive wear resistance of CoB/Co2B coatings formed in CoCrMo alloy , *Surface & Coatings Technology* **284** (2015) 258-263. `https://doi.org/10.1016/j.surfcoat.2015.06.081`.

37. J. L. Arguelles-Ojeda *et al.*, Corrosion behavior of boride diffusion layer on CoCrMo alloy Surface , *Indian Journal of Engineering and Materials Sciences* **27** (2020) 87-95.